Effect of plate slope and water jetting on the penetration depth of a jack-up spud-can for surficial sands

Dong-Seop Han[*1], Seung-Jun Kim[2] and Moo-Hyun Kim[2]

[1]*Research Institute of Green Energy Equipment, Dong-A University, Busan, 604-714, Korea*
[2]*Coastal and Ocean Engineering Division, Zachry Department of Civil Engineering,
Texas A&M University,College Station, Texas, 77843, USA*

Abstract. The spudcan requires the suitable design considering the soil, platform, and environmental conditions. Its shape needs to be designed to secure sufficient reaction of soil so that it can prevent overturning accidents. Its shape also has to minimize the installation and extraction time. Even in the same soil condition, the reaction of soil may be different depending on the shape of spud can, mainly the slope of top and bottom plates. Therefore, in this study, the relation between the slope of plates and the reaction of soil with and without water jetting is analyzed to better understand their interactions and correlations. For the investigation, a wind turbine installation jack-up rig (WTIJ) is selected as the target platform and the Gulf of Mexico is considered as the target site. A multi layered (sand overlying two clays) soil profile is applied as the assumed soil condition and the soil-structure interaction (SSI) analysis is performed by using ANSYS to analyze the effect of the slope change of the bottom plate and water jetting on the reaction of soil. This kind of investigation and simulation is needed to develop optimal and smart spudcan with water-jetting control in the future.

Keywords: jack-up platform; spudcan; top and bottom plates; soil-structure interaction model; punch through; peak resistance; water jetting; structural design; finite element analysis

1. Introduction

The spudcan is at the bottom of jack-up legs and used for temporarily fixing a jack-up platform on seabed. It largely consists of sloped top and bottom plates and side walls, which requires the suitable design considering the soil, platform, and environmental conditions. During the installation, operation, and extraction processes, if there is not enough resistance force and moment by soil, it can lead to the overturning accidents. To prevent this kind of accident, a spudcan should be inserted up to sufficient depth so that the whole structure can be supported by the sufficient resistance of soil (e.g., DNV codes (2012)). On the other hand, the speed up of lowering and extracting processes is also important to reduce the operational cost. So, the spudcan must be designed not only to secure the proper reaction force and moment from soil but also to minimize the installation/extraction time.

Even in the same soil condition, the reaction forces from soil may be different depending on the

---

∗Corresponding author, Researcher, E-mail: imdshan@gmail.com

shape of spudcan, mainly the slope of top and bottom plates. If the slope is small, the resistance of soil can be increased but the installation and extraction processes take longer time. If the slope is large, the above processes can be fast but the resistance against external loadings may be reduced. Even after the shape of spudcan is determined, the water jetting system that can further reduce the installation/extraction time needs to be properly designed. The water jetting system also contributes to inserting a spudcan up to the required depth of soil. So, in order to optimize the shape of spudcan, the effect of the water jetting on the resistance of soil should also be considered (Han *et al*. 2014). Therefore, in this study, the relation between the slope of bottom plates and the reaction of soil is analyzed by indirectly considering the water-jetting effect during an installation process to better figure out the proper shape of spudcan.

For the investigation, a wind turbine installation jack-up rig (WTIJ) is selected as the target platform and the Gulf of Mexico (GoM) as the target site. The irregular wind and wave, and steady current recommended in API codes (2007) are applied as the environmental conditions and the external forces and moments at the connecting point between the leg and spudcan are calculated by using Charm 3D (Kang *et al*. 2012, Yang *et al*. 2011) and ABAQUS programs. Next, the change of soil's properties according to the water jetting time is simulated. Lastly, multi layered (sand overlying clay) soil profile is applied as soil condition, and the soil-structure interaction (SSI) analysis is performed by using ANSYS (2012) to analyze the effect of the spudcan slope and water jet on the reaction of soil. For this purpose, slope angles of bottom plate are used as the primary design parameter (Tho *et al*. 2012, Yu *et al*. 2012).

2. Loading analysis

2.1 Target platform

A jack-up wind turbine installation vessel (WTIV) typically has 4~6 legs and is operated in water depth within 100 m. The WTIV selected here as the target platform has 6 legs and is operated in the water depth of 75 m. Fig. 1 shows the schematic view of the wind turbine installation vessel including 6 legs. The total vertical structural loading of it is about 440 MN including the weight of cranes, storage and water-ballast tanks. The maximum static vertical force occurs on the spud-can attached in a right-rear leg and its magnitude is 80.35 MN. This is selected as the target spud-can.
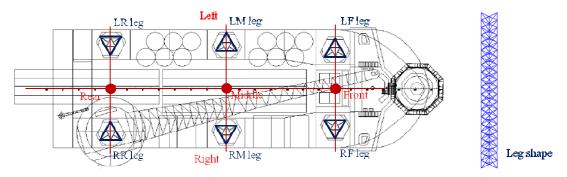

Fig. 1 Schematic of the wind turbine installation vessel (WTIV) and a leg

2.2 Environmental loadings

In order to simulate the structural behavior of the WTIV platform under the specific environmental condition, wind, wave, and current presented by API code were applied.

Wind Wind-velocity time-series can be generated based on the wind power spectrum presented by API wind spectrum, the spectral energy density ($s(f)$) at frequency (f) is described as below

$$S(f) = 320 \left(\frac{U_0}{10}\right)^2 \left(\frac{z}{10}\right)^{0.45} \Big/ \left(1 + \tilde{f}^n\right)^{(5/3n)} \tag{1}$$

$$\tilde{f} = 172 f \left(\frac{z}{10}\right)^{2/3} \left(\frac{U_0}{10}\right)^{-0.75} \tag{2}$$

where n=0.468, z is the height above sea level, U_0 is the 1-hour mean wind speed at 10m above sea level. In this study, it is assumed that the platform is installed and operated at West region of GoM, so 39.9 m/s of 1-hour mean wind speed is considered as the 100-y return period wind. According to the general equation of wind force, the wind-force time series applied to the exposed surface (F_W) can be calculated as follows

$$F_W = CqS \sin\theta \tag{3}$$

where C is the shape coefficient (C=1.28 for flat plate), q is the wind pressure ($q=1/2\rho_\alpha U^2{}_{T,z}$), ρ_α is the mass density of air, $U_{T,z}$ is the normal wind velocity at time (T) and at a height (z) above the mean sea level, S is the projected area of the member normal to the direction of the force, and θ is the angle between the direction of the wind and the axis of the exposed projected area.

Wave&current For wave loading estimation, JONSWAP spectrum with peak enhancement factor =2.4 is used to simulate the time-series of irregular sea-surface elevations. As mentioned previously, it is assumed that the WTIV platform is installed and operated at West region of G.O.M. Table 1 shows the parameters applied to the wave spectrum (West G.O.M, 70 m mean sea level, 100y return period hurricane event), based on the API code. Also, according to the API code, current velocity at West G.O.M under 100y return period hurricane is 1.31 m/s uniformly applied up to 70.0 m depth.

For the normal component (q_n) of the distributed external force acting on the rod per unit length, the following equation is used based on the equation of generalized Morison equation
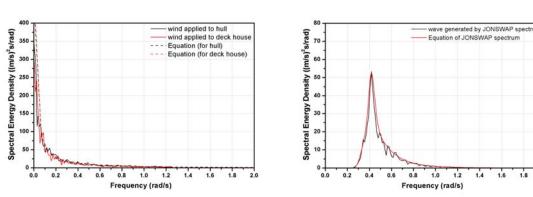
$$q_n = C_I \rho A_e \dot{v}_n + C_D \tfrac{1}{2} \rho D_s |v_{nr}| v_{nr} + C_m \rho A_e \ddot{r}_n \tag{4}$$

where C_I, C_D, and C_m are inertia, drag, and added mass coefficients, and $\dot{v}_n$, v_{nr}, and $\ddot{r}_n$ are normal fluid acceleration, normal relative velocity, and normal structure acceleration, respectively. The symbols ρ, Ds and A_e in the equation are fluid density, local diameter, and outer cross sectional area, respectively (Kim and Chen 1994, Kim and Ran 1994).

Fig. 2 shows the wind-velocity and wave-amplitude spectra generated by CHARM3D program for API spectrum and JONSWAP spectrum. The respective time histories were first generated from the input theoretical spectra for time-domain simulations. The respective spectra were also regenerated from the time series and compared with the input spectra for double checking purpose.

Table 1 Parameters for simulation of wave elevation

Items	Values
Significant wave height (*m*)	11.2
Peak period (*s*)	15.1
Enhancement factor	2.4

(a) wind energy density   (b) wave energy density

Fig. 2 Comparison of the wind and wave spectrum generated by CHARM3D program and API spectrum and JONSWAP spectrum

Combination of wind, wave, and current loads The time-series of environmental loadings on all the members due to wave, wind, and current in 70 m mean water level were calculated by using the Charm3D program considering various cases such as peak wave, peak wind, and peak current cases in the operation and installation conditions. With the environmental conditions, the forces applied on the spudcan are obtained by using ABAQUS. Table 2 shows the environmental forces on the spudcan in peak wave, peak wind, and peak current cases. By using the random wind and wave inputs, the wind and wave forces were simulated for the given platform and environmental cases.

Table 2 The environmental forces applied on the spudcan in peak wave, peak wind, and peak current cases (current direction=0º)

Load cases	Forces(*kN*)			Moment(*MN-m*)
	Fx (Longitudinal)	Fy (Transverse)	Fz (Vertical)	Mx(Overturn)
Peak wind (wind/wave angle=15º)	344	1,701	-82	-66.7
Peak wave (wind/wave angle=15º)	474	2,777	-82	-103.1
Peak Current (wind/wave angle=0º)	3	1,480	-83	-50.1

In this study, the additional dynamic vertical loading (Fz) applied on the spudcan is only considered because the slope of the bottom plate is mainly related with the vertical loading during the lowering process. Accordingly, the required vertical reaction of soil is 80.45 MN when considering both structural weight (80.35 MN) and 1.2-times environmental loading (83 kN) i.e., the additional dynamic loading in the z direction is small compared to the weight of the structure. In an independent analysis, the resistance from the soil for the corresponding horizontal shear and over-turning moment is found to be sufficient if the submergence depth is greater than half of the spudcan height.

3. Soil-structure interaction (SSI) analysis

3.1 Basic theory

Mohr-Coulomb model Shear stress of soil in Mohr-Coulomb (MC) failure criterion is expressed as below

$$\tau = c + (\sigma_n - u)\tan\varphi \tag{5}$$

where c is the cohesion, σ_n is the overburden pressure on the soil element ($\sigma_n = \gamma_d D$), u is the pore water pressure within the soil element, φ is the internal friction angle of soil, γ_d is the soil's submerged unit weight, and D is the embedment depth.

Extended Drucker-Prager (EDP) theory The extended Drucker-Prager (EDP) material model includes yield criteria and corresponding flow potentials similar to those of the classic Drucker-Prager model commonly used for geomaterials with cohesion and internal friction. The EDP linear-yield criterion can be expressed as below (Kai *et al.* 2009)

$$t = p\tan\beta + d \tag{6}$$

where t is the deviatoric stress, $p = (\sigma_x + \sigma_y + \sigma_z)/3$, $d = (1 - tan\beta/3)\,\sigma_{yc}$, and $\tan\beta = 3\sqrt{3}\alpha$, $d = \sqrt{3}\kappa$. Then, the material parameters of soil α and κ in Drucker-Prager (DP) model can be obtained as follows

$$\alpha = \frac{2\sin\varphi}{\sqrt{3}(3-\sin\varphi)}, \qquad \kappa = \frac{6c\cos\varphi}{\sqrt{3}(3-\sin\varphi)}$$

The EDP linear plastic flow potential form can be expressed as below

$$t = p\tan\beta' \tag{7}$$

where $\tan\beta' = 3\sqrt{3}\alpha'$ and $\alpha' = \dfrac{2\sin\psi}{\sqrt{3}(3-\sin\psi)}$, ψ is the dilation angle.

3.2 Water jetting effect

Water jetting is frequently used to speed up the installation and extraction of the jack-up spudcan. When water jetting is operated, the pore pressure of the region near water nozzles is changed, and the changed pore pressure and the seepage force affect the effective vertical soil

pressure. So, the shear strength of soil varies due to the change of the effective vertical pressure, as shown in Eq. (5). In other words, if the changes of the pore pressure and seepage force are theoretically estimated, the change of shear strength of soil can be determined. As for SSI analysis, the effect of the pore-pressure and seepage-force changes on the shear strength can be more simply considered by applying the equivalent internal friction angle, as suggested by Duan *et al*. (2013). Since other parameters, such as cohesion, friction coefficient, etc., also change due to the water jetting, the actual physics can be more complicated and the current model is a simplified one. However, our independent sensitivity study reveals that the sensitivity with other parameters is relatively less important. In this regard, to consider the change of shear strength of sand soil due to water jetting, the equivalent internal friction angles are calculated by the equations suggested by Duan *et al*. (2013). Then, they are subsequently applied to the material property of the sand models as requested by ANSYS for SSI analysis. The equivalent internal friction angle (φ') of the sand layer at time t is expressed as below

$$\varphi' = \arctan\left(\frac{\sigma_n - u - f}{\sigma_n - u_0}\tan\varphi\right) \tag{8}$$

where σ_n is the overburden pressure

$$\sigma_n = u_0 + \frac{Q_f}{\pi D_o H \tan\varphi}$$

u is the pore pressure due to jetting time t

$$u = u_0 + \frac{q\gamma_w R(t)}{2\pi k h (R(t) - R_w)}\left[\ln\frac{r}{R(t)} - \frac{r}{R(t)} + 1\right] \qquad R_w \leq r \leq R(t)$$

f is the seepage force at jetting time t

$$f = -\frac{q\gamma_w R(t)}{2\pi k h (R(t) - R_w)}\left[\frac{1}{r} - \frac{1}{R(t)}\right]$$

where u_0 is the initial pore pressure, Q_f is the bearing capacity of the subsoil, q is the jetting rate of a nozzle, $R(t)$ is the disturbed zone, R_w is the radius of a nozzle, r is the distance between the *i-th* nozzle and point $M(r, \theta)$, D_o is the diameter of spudcan, H is the depth of the overlaid thin sand layer, k is the permeability coefficient, and h is the thickness of seepage layer.

Substituting the conditions into the analytic model (8), the equivalent angle of internal friction due to water jetting can be estimated with respect to the jetting time t. Fig. 3 shows the effect of water jetting on the change of the equivalent internal friction angle of sand layer with time and flow rate. As shown in Fig. 3, the equivalent angles of internal friction are reduced to 25 deg (when Q=240 m³/h) and 22 deg (when Q=320 m³/h), respectively, from the initial value of 30 deg. after 36 hours. As can intuitively be expected, multi-nozzles are more effective than single nozzle in decreasing equivalent internal friction angle. Also, higher flow rates produce bigger decrease in equivalent internal friction angle.

3.3 Analytical/Numerical spudcan-soil model

Spudcan modeling The spudcan selected here consists of an approximated inverted cone with maximum diameter of 12.0 m and height of tip to base 2.7~4.1 m with the range of bottom-plate slope 0-15 degrees. Asa design parameter, six slope angles of bottom plate (2.5, 5.0, 7.5, 10.0, 12.5,

15.0 degrees) are considered. Its material is steel that behaves elastically. Fig. 4 shows the schematics of the spudcan.

   Soil Modeling The initial profile of soil is given by Table 3. There are three soil layers (surficial sand and two clays below it) based on a specific site of GoM. The friction coefficient μ between the spudcan surface and soil is set up as 0.3. The Elastic modulus (E) is taken approximately $4×q_c$ (for sand) and $200×C_u$ (for clay), where q_c is the tip resistance from the CPT data and C_u is the undrained shear strength of clay. Poisson's ratios (ν) are0.3 (for sand) and 0.49 (for clay), respectively. The dilatation angle (ψ) for sand is equal to the internal friction algle (φ) for the Mohr-Coulomb (MC) model. The Drucker-Prager (DP) model is derived from the MC model. In this study, Extended Drucker-Prager (EDP) model is used (Zhao *et al*. 2011).
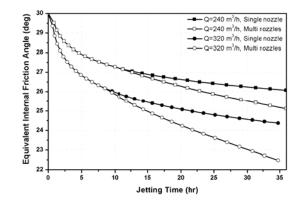

Fig. 3 Jetting effect of nozzles on the change of internal friction angle of the sand layer (when *k* = 5E-5 m/s, R_w= 0.3 m)
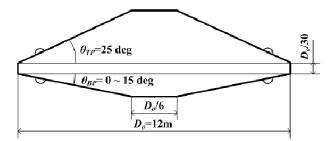

Fig. 4 Schematics of the spudcan

Table 3 Initial profile of soil

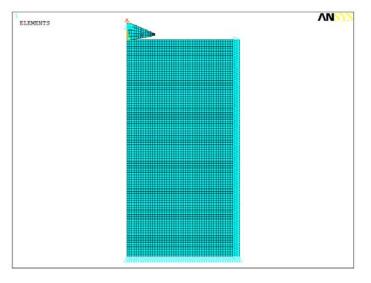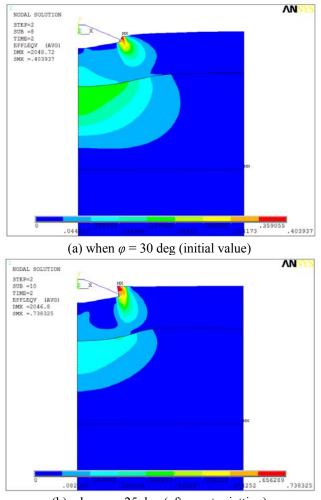| Soil type	Depth(*m*)	Submerged unit weight(kN/m^3)	Undrained shear strength (*kPa*)	Cohesion (*kPa*)	Internal friction angle (*deg*)
SAND	0 - 5.85	9.0	NA	10	30
CLAY(firm)	5.85-19.5	8.7	50	30	0
CLAY(stiff)	19.5-46.3	8.8	80	30	0

Fig. 5 Meshed shape and boundary condition for SSI analysis

Soil-structure interaction(SSI) modeling The soil-spudcan interaction is simulated by the surface-to-surface contact pair interaction. The spudcan is selected as a contact surface and the soil as a target surface. The friction coefficient is taken as 0.3 for the contact between sand and the spudcan. With water jetting, the friction coefficient may vary but the result is not that sensitive to its change. Radial directional d.o.f (ux) of nodes on the side line of soil and vertical directional d.o.f (uy) of nodes on the bottom line of soil are fixed, respectively. The vertical displacement (uy) of top of spudcan is pulled down to 5 m vertically, after applying the acceleration of gravity. Fig. 5 shows the meshed shape and boundary condition for soil-spudcan interaction model (Kellezi *et al*. 2003 and Qiu *et al*. 2012). In this study, the Soil-Structure Interaction (SSI) analysis is based on the implicit finite element method produced by ANSYS, for which the Lagrangian (L) formulation is supported for a mesh solution. When the deformation is very large, the difference between the L formulation and Arbitrary Lagrangian-Eulerian (ALE) formulation may be increased, so if high accuracy is needed, ALE approach is preferred. However in this study, the spud-can penetration to the sand is typically small, so the results are to be reasonable for that purpose.

3.4 Results of SSI analysis

The soil-spudcan interaction analysis was carried out by using ANSYS program. The 2D-axisymmetric model for the soil-spudcan is used as analysis option. Fig. 6 shows the equivalent plastic strain distribution of three layers of soil when the slope angle of bottom plate is 10 deg and penetration depth is 2 m. As shown in Fig. 6, shear failure occurs in the first layer (sand) and the second layer (firm clay) is compressed but the third layer (stiff clay) is little affected, while the spud-can penetrates the soil into 2 m-depth. Also, the equivalent plastic strain of the sand layer increases two times, when the internal friction angle of sand layer is reduced from 30 deg to 25 deg due to water jetting.

(a) when φ = 30 deg (initial value)

(b) when φ = 25 deg (after water jetting)

Fig. 6 Equivalent plastic strain distribution of soil when the penetration depth is 2 m (θ_{BP} = 10 deg)

4. Results and discussions

4.1 Effect of slope change of bottom plate

To evaluate the effect of the bottom-plate slope angle on the penetration resistance of a soil, the SSI analysis is carried out for six slope angles (0 to 15 degrees). Fig. 7 shows the penetration resistance of soil depending on the bottom-plate slope angle.

In Fig. 7, the initial penetration before the 1st punch-through point, which is defined by rapid change of curve slope, is due to the compressive deformation of a soil. The rapid drop after the 1st punch-through point is due to the shear failure/fracture of the first layer (sand) triggered at the spud-can side edge. The range of drop increases with the increase of bottom-plate angle. After

further penetration, the soil resistance reaches a peak value and cannot sustain any more weight after that. In summary, with larger bottom-plate angle, the penetration can be deeper and easier but it may also pose a risk associated with large punch-through-failure range before reaching maximum soil resistance.

To see the trend in more detail before reaching the 1st punch-through point, Fig. 8 plotted the relation between the bottom-plate slope angle and the resistance of a soil in that range.

The penetration depth at each penetration resistance is plotted as function of bottom-plate slope angle. When the vertical loading is 60 MN, the curve is almost a straight line (linear behavior). If load is less than that the depth increase rate becomes smaller with larger angle. If load is larger than that the depth increase rate becomes greater with larger angle (convex curve).

Next, to analyze the relation between the bottom-plate slope angle and the resistance of a soil after the 1st punch-through point, the 1st punch-through point and peak resistance point are given in Fig. 9 as function of bottom-plate slope angle. And Table 4 shows the linear fitting results for 1st punch-through and peak resistance of soil according to the bottom-plate slope angle.
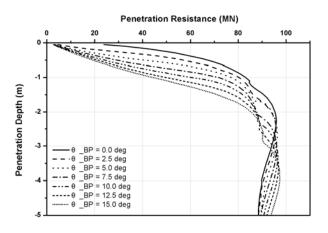

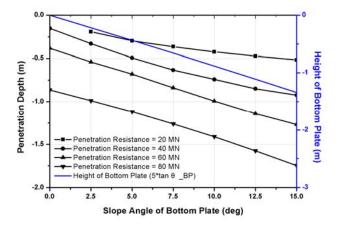Fig. 7 Penetration resistance of soil according to the slope angle of bottom plate

Fig. 8 Penetration depth as function of bottom-plate slope angle for each penetration resistance
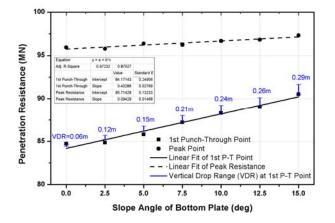
Fig. 9 Comparison of punch-through and peak resistance of the spudcan according to the slope angle of bottom plate

Table 4 Linear fitting results for 1st punch-through and peak resistance of soil according to the slope angle of bottom plate (θ_{BP})

Items	Y=A+Bθ_{BP}		Relation coefficient
	A (intercept)	B (Slope)	
1st Punch through	84.171	0.403	0.972
Peak Resistance	95.714	0.094	0.870

In the figure, the value of 1st punch-through point increases from 84.7 to 90.5 MN as the slope angle of bottom plate increases from 0 to 15 degrees but the values of peak resistance point do not change much and remain in the range of 95.9 ~ 97.3 MN. The corresponding slopes of the linear fitting lines of two cases are about 0.4 and 0.1, respectively, as shown in Table 4. The slope change of bottom plate strongly affects the 1st punch-through point but it has little effect on the soil peak resistance. The range of vertical drop during the 1st punch-through process is also marked in Fig. 9. The given numbers are for true vertical drop and if near-vertical drop is also considered, the range is appreciably increased. We see larger drop with larger plate angle. The larger vertical drop by punch through means higher risk during installation process. Therefore, the increase of bottom-plate slope has both pros and cons. The mechanism of punch-through process is mainly caused by shear fracture at the side edge of spud-can, so it is closely connected to the corner angle i.e., slope of bottom plate.

By the way, when the resistance of soil is 80.45 MN (that is the maximum vertical loading applied on a spudcan), the penetration depths depending on the bottom-plate angle are -0.88 ~ -1.77 m. In case of surficial sand, this kind of shallow-penetration problem is well known to spud-can designers. The spudcan with outer diameter of 12 m can support the vertical loading of

80.45 MN but the corresponding shallow penetration depths may not be enough to prevent overturning in harsh environments. Also, scour may cause additional problem. So, a water jetting system may be needed to insert the spudcan up to the required depth to avoid those problems.

4.2 Effect of water jetting through bottom plate

As mentioned in the previous section, due to the water jetting, the pore pressure/seepage force is changed and that can be represented by the change of internal friction angle. So, three internal friction angles (30, 27, and 25 degrees) are adopted as the design parameter for four bottom-plate angles of (0, 5, 10, 15 degrees) to evaluate the effect of water jetting on the penetration resistance of soil. The 25-degree internal friction angle corresponds to the water-jetting case of 240/320 m^3/h by multi nozzles after 35/15 hours. The peak penetration-resistance change of soil due to the water jetting for each bottom-plate angle is shown in Fig. 10 and Table 5.
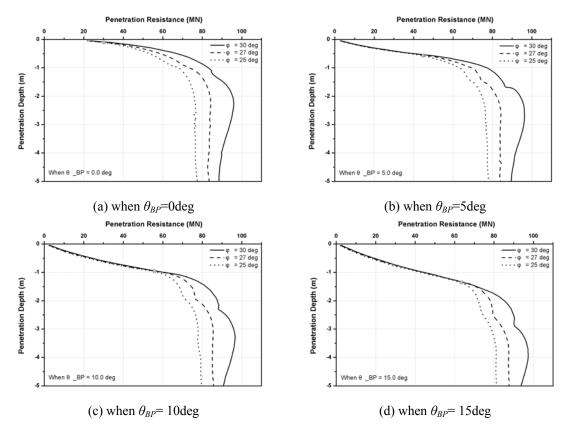

(a) when θ_{BP}=0deg

(b) when θ_{BP}=5deg

(c) when θ_{BP}= 10deg

(d) when θ_{BP}= 15deg

Fig. 10 Penetration resistance change of soil due to water jetting for various angles of bottom plate

Table 5 Peak resistance of soil according to the slope angle of bottom plate and the internal friction angle

Slope angle of bottom plate (*deg*)	Peak Resistance (*MN*)		
	30 deg w/o water jetting	27 deg with water jetting	25 deg with water jetting
0.0	95.9	84.2	76.2
5.0	96.4	84.3	76.5
10.0	96.7	85.5	77.7
15.0	97.3	87.5	81.1

As shown in Fig. 10, if the internal friction angle of sand is decreased by using the water jetting system, the spud-can can penetrate deeper regardless of bottom-plate slope angles for platform weight close to 80 MN. However, the peak resistance of soil is also reduced as a result of water jetting, so may be vulnerable to major punch-through instability having near-vertical slope if the water jetting time is too long. In such a case, it has to be stopped before the soil resistance approaches its peak value. In case of lighter platforms, we can see more water-jetting effect when the bottom-plate angle is smaller. From the above results, we can conclude that the water-jetting generally helps the spud-can to penetrate deeper but its effect is not that significant in the case of surficial sands, which has been experienced in the real cases.

The principal purpose of using the water jetting in surficial sand condition is to insert the spudcan up to the required depth. As shown in Table 5, as the slope angle of bottom plate increases from 0 to 15 degrees, the corresponding reduction ratio for the peak resistance decreases from 20.5 to 16.6%. The reason why the effect becomes smaller for larger angle is that the angle between bottom plate and side wall of a spudcan increases and it makes the shear fracture weaker. Accordingly, the effect of water jetting is more as the slope angle of bottom plate decreases.

To see the effect of soil properties on the penetration resistance of a soil, the SSI analysis is carried out for six different combinations of sand-layer properties as shown in Table 6. Fig. 11 shows the change of penetration resistance of soil for varying cohesion, friction coefficient, and internal friction angle when the slope angle of bottom plate is 10 degrees.

Table 6 Combination of soil property for a sand layer

Combination No.[†]	Sand layer		Friction coef. between sand and spudcan(μ)
	Internal friction angle(φ) (*deg*)	Cohesion(c) (*kPa*)	
NWJ-01	30	10	0.3
NWJ-02	30	5	0.3
NWJ-03	30	10	0.2
WJ-01	25	10	0.3
WJ-02	25	5	0.3
WJ-03	25	10	0.2

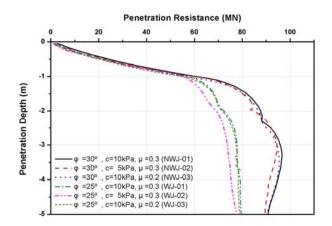† NWJ : Non Water Jetting State, WJ : Water Jetting State

Fig. 11 Penetration resistance of a soil according to the soil properties when the slope angle of bottom plate is 10 deg

In Fig. 11, for both water-jetting case and without it, the final results are not significantly different from the original results with the given typical values, which means that small variations of soil properties by water jetting do not significantly alter the general trend and conclusions of the previous sections.

Finally, the water-jetting may also reduce the structure-soil resistance against shear loading and overturning moment. To see the effect, the SSI analysis for the 3D model with the bottom-plate angle of 10 deg is carried out for six internal friction angles (30 to 25 degrees with 1-deg interval). Fig. 12 shows the change of overturning and horizontal resistance of a soil according to the internal friction angle when the vertical resistance of a soil is reached at 80.45MN.

(a) overturning resistance of soil

(b) horizontal resistance of soil including friction by weight with riction coefficient=0.1
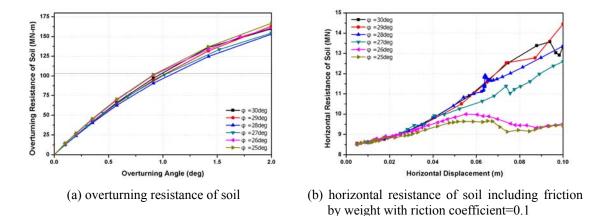
Fig. 12 Overturning and horizontal resistance of a soil with varying internal friction angle when the vertical resistance of soil is reached at 80.45MN

In Fig. 12, all the cases can sufficiently resist the present maximum shear forces 2.78MN and maximum overturning moment 103.1MN-m(see Table 2). The maximum overturning moment corresponds to 1-degree spud-can angular deformation. In general, the resistance capability of soil against shear loading significantly decreases with more water jetting. The change of resistance against shear loading is much more sensitive than that for overturning moment. When the platform is relatively less heavy, the significant reduction against the shear loading can be a problem. However in the present case, the resistance against such loadings is sufficient regardless of water-jetting.

5. Conclusions

In this study, soil-spudcan interaction analysis is carried out to evaluate the effect of slope angle of bottom plate and water jetting on the penetration resistance of soil.

In case of a spudcan with outer diameter of 12 m, a punch-through process occurs over 84.7 MN and the peak resistance of soil is around 96 MN regardless of the slope of bottom plate. The spudcan can generally support the required vertical loading of 80.45MN in sand but the penetration depth is not sufficient without water jetting. So, water jetting is needed to insert the spudcan up to the required depth. When the slope angle of bottom plate increases, the resistance curve (bear capacity) of soil is gradually reduced without water jetting, so it can penetrate deeper. However, the fall range of 1st punch through point is also significantly increased to pose a higher risk associated with installation process. With water jetting, the equivalent internal friction angle of sand is decreased, so the spudcan can be penetrated deeper. However, the peak resistance of soil is reduced and it needs to be stopped when the soil resistance approaches the point. The water-jetting process may also reduce the soil resistance against the shear loading and overturning moment on the structure, so a careful checking is needed. This kind of numerical simulation is necessary to better understand the overall physics and develop optimal and smart spudcan with water jetting control in the future.

Acknowledgements

References

American Petroleum Institute (2007), *API BULLETIN 2INT-MET Interim Guidance on Hurricane Conditions in the Gulf of Mexico*, Washington, D. C., U.S.A.
ANSYS, Inc. (2012), *ANSYS Mechanical APDL Material Reference*.
Det Norske Veritas AS (2012), *Self-elevating Units*.
Duan, M., Zhao, J., Wang, J. and Song, L. (2013), "*Jetting* effect of jackup on actively punching through overlaid sand layer", *Int. J. Offshore Polar.*, **23**(1), 55-62.
Kai, S.U. and Yin, L.I. (2009), "Discussion of extended drucker-prager yield criterion in slope stability analysis", *Proceedings of the Power and Energy Engineering Conference*, 2009 APPEEC.
Kang, H.Y. and Kim, M.H. (2012), "Hydrodynamic interactions and coupled dynamics between a

container ship and multiple mobile harbors", *Ocean Syst. Eng.*, **2**(3), 217-228.

Kim, M.H. and Chen, W. (1994), "Slender body approximation for slowly-varying wave loads in multi-directional waves", *Appl. Ocean Res.*, **16**(3), 141-163.

Kim, M.H. and Ran, Z. (1994), "Responses of an articulated tower in waves and currents", *Int. J. Offshore Polar.*, **4**(4), 298-391.

Kellezi, L. and Stromann, H. (2003), "FEM analysis of jack-up spudcan penetration for multi-layered critical soil conditions", *Proceeding of BGA International Conference on Foundations*.

Han, D.S., Kim, S.J., Kim, M.H. and Park, Y.C. (2014), "Relation between slope of plate and reaction of soil in a spudcan for jack-up platform", *Proceedings of the International Offshore and Polar Engineering*

Qiu, G. and Grabe, J. (2012), "Numerical investigation of bearing capacity due to spudcan penetration in sand overlying clay", *Can. Geotech. J.*, **49**, 1393-1407.

Tho, K.K., Leung, C.F., Chow, Y.K. and Swaddiwudhipong, S. (2012), "Eulerian finite-element technique for analysis of jack-up spudcan penetration", *Int. J.* Geomech. - ASCE, **12**(1), 64-73.

Yang, C.K. and Kim, M.H. (2011), "The structural safety assessment of a tie-down system on a tension leg platform during Hurricane events", *Ocean Syst. Eng.*, 1(4), 263-283.

Yu, L., Hu, Y., Liu, J., Randolph F.M. and Kong, X. (2012), "Numerical study of spudcan penetration in loose sand overlying clay", *J. Comput. Geotech.*, **46**, 1-12.

Zhao, J., Duan, M., Cao, S., Hu, Z. and Song, L. (2011), "Prediction of spudcan penetration depth in multiple layers with sand overlying clay", *J. Appl. Mech. Mater.*, **52-54**, 995-1002.